Temperature and water vapor variance scaling in global models: Comparisons to satellite and aircraft data

B. H. Kahn[1], J. Teixeira[1], E. J. Fetzer[1], A. Gettelman[2], S. M. Hristova-Veleva[1], X. Huang[3], A. K. Kochanski[4], M. Köhler[5], S. K. Krueger[4], R. Wood[6], and M. Zhao[7]

[1] Jet Propulsion Laboratory, California Institute of Technology, Pasadena, CA, USA

[2] National Center for Atmospheric Research, Boulder, CO, USA

[3] Department of Atmospheric, Oceanic and Space Sciences, University of Michigan, Ann Arbor, MI, USA

[4] Department of Atmospheric Sciences, University of Utah, Salt Lake City, UT, USA

[5] Deutscher Wetterdienst, Offenbach, Germany

[6] Department of Atmospheric Sciences, University of Washington, Seattle, WA, USA

[7] Geophysical Fluid Dynamics Laboratory, Princeton, NJ, USA

Submitted to *J. Climate* on October 15th, 2010

Corresponding author:

Brian H. Kahn
Jet Propulsion Laboratory
4800 Oak Grove Drive,
Mail Stop 169-237,
Pasadena, CA 91109
Tel (818) 393–0676
Fax (818) 393–4619
Brian.H.Kahn@jpl.nasa.gov

Abstract

Observations of the scale dependence of height-resolved temperature (T) and water vapor (q) variability are valuable for improved subgrid-scale climate model parameterizations and model evaluation. Variance spectral benchmarks for T and q obtained from the Atmospheric Infrared Sounder (AIRS) are compared to those observed by state-of-the-art numerical weather prediction and climate model "analyses" or "free-running" simulations with spatial resolution comparable to AIRS. The T and q spectra from both types of models are generally too steep such that small-scale variance is up to several factors smaller than AIRS. However, the two model analyses more closely resemble AIRS than the two free-running model simulations. Scaling exponents obtained for AIRS column water vapor (CWV) and height-resolved layers of q are also compared to the super-parameterized Community Atmospheric Model (SP-CAM) that highlight very large differences between CWV and height-resolved q scaling characteristics. Height-resolved q spectra obtained from aircraft observations during the Variability of the American Monsoon Systems Ocean-Cloud-Atmosphere-Land Study Regional Experiment (VOCALS-REx) demonstrate changes in scaling exponents that depend on the observations' proximity to the base of the subsidence inversion with scale breaks that occur at approximately the dominant cloud scale (~10–30 km). This suggests finer spatial resolution requirements must be considered in future satellite observations of T and q than those currently planned for infrared and microwave satellite sounders.

1. Introduction

The scale dependences of atmospheric horizontal winds, potential temperature (θ) and kinetic energy (*KE*) power spectra obtained from aircraft observations follow an approximate –3 power law wave number scaling for length scales > 800 km (and –5/3 for scales < 500 km) (e.g., Nastrom and Gage, 1985), but a complete physical explanation of their origin remains vigorously debated (e.g., Tung and Orlando, 2003; Tulloch and Smith, 2006; Lindborg, 2009; Lindborg et al., 2009; Lovejoy et al. 2009; Smith and Tulloch, 2009; Tuck, 2010). Observational benchmarks of scaling exponents have been used to evaluate *KE* spectra obtained from relatively low (Koshyk et al*.,* 1999) and high (Skamarock, 2004; Takahashi et al., 2006; Hamilton et al., 2008) resolution NWP and climate models in order to gain insights on model physics and determine whether the –3 to –5/3 break in the mesoscale region is faithfully represented.

Most of the emphasis to date in the literature focuses on comparisons of *KE* spectra between observations and models (Hamilton et al*.*, 2008). The scale dependences of the variability of temperature (*T*) and especially water vapor (*q*) are not well characterized in space and time on a global basis, despite both variables strongly controlling cloud processes at the subgrid-scale in NWP and climate models (Cusack et al., 1999; Tompkins, 2002; Wang et al., 2010) and, therefore, help to establish the sign and magnitude of cloud feedbacks (Randall et al*.*, 2007). Furthermore, the few existing aircraft studies of *q* spectra in the mesoscale (e.g., Nastrom et al*.*, 1986; Cho et al., 2000)

support an approximate –2 scaling with little or no mesoscale break reported, in stark contrast to potential temperature and *KE* spectra.

Recently, Kahn and Teixeira (2009; herein KT09) obtained a global observationally based climatology of T and q variance scaling derived from the Atmospheric Infrared Sounder (AIRS)/Advanced Microwave Sounding Unit (AMSU) (hereafter "AIRS") suite between ~150–1300 km. A rich variety of structure in the scaling exponents was revealed from these observations that were not previously reported from aircraft (e.g., Nastrom and Gage, 1985) and satellite observational studies (e.g., Cahalan et al., 1994) owing to aircraft sampling limitations, and ambiguities in interpreting raw satellite radiances (KT09). Geophysical products obtained from satellite sounders and imagers are potentially very powerful because of their ability to represent a scale-dependent probability distribution function (PDF) over, potentially, orders of magnitude in spatial scale, depending on the sensor spatial resolution and swath characteristics, with near global sampling coverage. Furthermore, it is the scale dependence of joint PDFs of T and q that dictate the distributions of cloud condensate (e.g., Kawai and Teixeira, 2010; Wang et al., 2010) and climate sensitivity (e.g., Kuwano-Yoshida et al., 2010).

In this paper, scaling exponents derived from AIRS, two contemporary NWP model analyses, two "free-running" climate models, one "super-parameterized" climate model, and aircraft data from the Variability of the American Monsoon Systems Ocean-Cloud-Atmosphere-Land Study (VOCALS) Regional Experiment (VOCALS-REx) (Wood et al., 2010) are described, where AIRS and model horizontal resolutions are comparable. Although many published aircraft-based turbulence spectrum studies exist,

especially with regard to the free troposphere (e.g., Nastrom and Gage, 1985), the present paper emphasizes VOCALS-REx data within stratocumulus because of its large potential contribution to cloud-climate feedback (Bony and Dufresne, 2005). We will show that the climate and NWP models evaluated herein tend to under-estimate small-scale variance of T and q, but important differences exist among them in relation to data assimilation, initialization and subgrid-scale parameterizations.

2. Model and observational data

The AIRS on EOS Aqua has observed up to 324,000 vertical profiles of T and q on a daily basis since September 2002 (Aumann et al. 2003). The retrieval approach is based on the cloud-clearing methodology (Susskind et al. 2003) and yields a nominal spatial resolution of about 45 km at nadir. The sampling, precision and quality control of T and q are discussed in KT09, Maddy and Barnet (2008), and elsewhere. The scaling exponents (0.33, 0.5, and 1.0 ≅ –5/3, –2, and –3, respectively) are obtained by fitting power laws to observed variance spectra of T and q within 12°×12° and smaller grid boxes and on tropospheric standard pressure levels following the approach in KT09. This grid size choice resolves the mesoscale range (1.5, 2.0, 3.0, 4.0, 6.0, and 12.0° scales) that contains the canonical –3 and –5/3 mesoscale break (Nastrom and Gage, 1985) but also resolves regional, latitudinal, and land/ocean variations. Separate exponents are obtained for the 1.5–4.0° (small) and 6.0–12.0° (large) scales. The large-scale exponent is fit to fewer points than in KT09, but comparisons between this approach and KT09 exhibit virtually no difference in the derived magnitude, and saves greatly on computational expense.

118 Results herein are restricted to relatively clear skies by retaining profiles only when the
119 AIRS total effective cloud fraction (ECF) < 0.1 (KT09). Important AIRS sampling
120 effects occur for larger values of ECF (Fetzer et al. 2006), in particular the lack of
121 sampling of temperature as well as high values of water vapor within thick clouds, which
122 may affect the interpretation of cloudy spectra. Therefore, the emphasis of this work is on
123 atmospheric conditions best sampled by AIRS observations.
124 As the resolution of the AIRS operational retrieval precludes the robust calculation
125 of variance < 150 km in scale, we also calculate T and q spectra observed at 1 s time
126 sampling during the VOCALS-Rex campaign (Wood et al. 2010) obtained from
127 meteorological instrumentation on the C-130 aircraft. To eliminate the confusion between
128 horizontal geophysical variability with altitude ($z_{C\text{-}130}$) ascents and descents through
129 strong vertical gradients, spectra of T and q are restricted to horizontally level flight
130 segments. Raw meteorological data from the C-130 were manually inspected for spurious
131 data and inversion base crossings and these were eliminated from further consideration.
132 Composite spectra are formed from calculating variance on flight segments of 4, 8, 16,
133 32, 64, 128, 256, 512, 1024, 2048, 4096, and 8192 s in time. With a nominal flight speed
134 of 100 ms^{-1}, this translates to distances of 0.4, 0.8, 1.6, 3.2, 6.4, 12.8, 25.6, 51.2, 102.4,
135 204.8, 409.6, and 819.2 km, respectively. The level flight tracks were composited into
136 five height categories of $z_{C\text{-}130}$ to reduce noise and geophysical variability: < 0.3, 0.3–0.7,
137 0.7–1.5, 1.5–3.0, and > 3.0 km. We obtain spectral exponents from composite spectra that
138 are calculated from averaging flight segments with length scales in between 102.4–204.8,
139 204.8–409.6, and 409.6–819.2 km that have at least five occurrences during VOCALS-
140 REx. There are very few flights with longer or shorter segments and, because of a small

141 sample size, these are less representative of the true geophysical variability of the
142 atmosphere and thus are not included. To illustrate the tendency for a change in the
143 scaling characteristics around the scales of the cloud features in the VOCALS-REx
144 region (e.g., Wood and Hartmann, 2006; Wood and Field, 2011), two spectral exponents
145 were separately obtained for scales less than and greater than 10 km.

146 Two free-running models are investigated. First, a modified version of the
147 Geophysical Fluid Dynamics Laboratory (GFDL) Atmospheric Model version 2.1
148 (AM2.1) with high spatial resolution is used following Zhao et al. (2009) (see Table 1 for
149 model details). The model is referred to as C180HIRAM2.1 and has a cubed sphere
150 dynamical core, with 180×180 grid points on each face of the cube, resulting in grid sizes
151 ranging from 43.5–61.6 km. In addition to changes in the dynamical core and spatial
152 resolution, the model also differs from GFDL's AM2 model (GAMDT 2004) in its
153 convection and cloud scheme (Zhao et al. 2009). Second, a modified version of the
154 National Center for Atmospheric Research (NCAR) Community Atmosphere Model
155 version 3 (CAM3) with high-resolution gridding (~0.31°×0.23°) is used (Gettelman et al.
156 2010). The newest version of the CAM3 includes a 2-moment microphysics scheme, an
157 updated rapid radiative transfer package, and improvements to the mixed and ice phases
158 of clouds are obtained by including ice supersaturation and ice cloud-aerosol interactions
159 at the point of ice nucleation. The scaling exponents of T and q are calculated as in KT09,
160 except the boxes are 12°×15° in the case of C180HIRAM2.1. A value of total cloud
161 fraction (CF) < 0.5 at TOA is used to screen for "clear-ish" skies, and little sensitivity of
162 this value is reflected in the scaling exponents. The ECF from AIRS and CF from the
163 model output are not equivalent since ECF is a convolution of cloud emissivity and

coverage, while CF > 0 simply indicates the presence of cloud. The relative frequency of occurrences of ECF < 0.1 and CF < 0.5 are similar in magnitude and sample relatively similar spatial regimes. Results from a free-running C180HIRAM2.1 simulation during 1 Sept 1995 – 30 Nov 1995 for 00 UTC snapshots, and a free-running CAM3 simulation from 1 June 2005 – 31 August 2005 for 00 UTC snapshots, are presented in Section 3.

Scaling exponents from two model analyses are also investigated. The first is the European Center for Medium range Weather Forecasting (ECMWF) (Jung et al., 2010) 00 UTC analysis fields provided on a 0.5°×0.5° grid as a part of the Year of Tropical Convection project. The model cycle is CY35R2 with a resolution of T799 (25 km) over 91 vertical levels. Several sources of data relevant to T and q are assimilated, which include Global Positioning System (GPS) occultations, radiosonde profiles, AIRS and Infrared Atmospheric Sounding Interferometer (IASI) radiances, as well as AMSU A/B and Special Sensor Microwave Imager (SSM/I) microwave radiances. The second model analysis is the Modern Era Retrospective Analysis for Research and Applications (MERRA) (http://gmao.gsfc.nasa.gov/merra/) fields at 1.25°×1.25° resolution. Note the native resolution of MERRA (version 5.2.0 of GEOS-5 DAS) is 0.5°×0.625°, similar to C180HIRAM2.1. GEOS-5 also assimilates many of the same data as ECMWF including radiosondes, AIRS, AMSU A/B, and SSM/I (Rienecker et al., 2008). As in the case of the C180HIRAM2.1 and CAM3 models, the T and q fields are restricted to CF < 0.5. Grid box sizes of 12°×12° (15°×15°) were used for ECMWF (MERRA) and results are presented below for 1 June 2009 – 31 August 2009 for both models.

Lastly, variance spectra of total column water vapor (CWV) and height-resolved q from the superparameterized CAM3 (SP-CAM) (Marchand et al. 2009) are compared to

CWV and q spectra obtained from AIRS and VOCALS-REx. Each GCM grid column of the SP-CAM is 2.5° in longitude × 2.0° in latitude and contains an embedded 2D cloud-resolving model (CRM) oriented in a W-E direction, with cyclic lateral boundary conditions within each GCM grid box. Each CRM contains 64 columns of 4 km horizontal grid size, and the variance is calculated at 8, 16, 32, 64, 128, 243, 487, 731, 975, and 1218 km once per day at 1200 UTC. The variance at scales less than 256 km is calculated from the 2D CRM fields only. Results are presented for two specific regions during 01 Sept – 30 Nov 1998, 1999, 2000, and 2001.

3. Results

3.1 Regional vertical profiles

Figure 1 illustrates model and AIRS variance spectra for T in three different cloud regimes: stratocumulus in the SE Pacific (SC), trade cumulus near Hawaii (TC), and a convectively active region in the tropical Western Pacific (DC). The magnitude of the AIRS T variance depends on altitude, length scale and region (KT09). The change in the slope of the variance (i.e., "scale break") at 500 hPa in SC is discernible around 400–600 km but is significantly weaker in TC and essentially non-existent in DC. A much weaker scale break is observed in the boundary layer and near the tropopause (KT09). Since the slope in the T variance is weaker at 925 hPa in SC, the relative magnitude compared to other pressure levels is significantly larger in DC showing large low-level T variability. There is a general tendency for the model spectral slopes to be uniformly steeper relative

210 to AIRS. This translates to *T* variance that is similar to or somewhat less than AIRS in
211 the 600–1300 km length scales, and several factors less than AIRS within the 150–400
212 km scales, depending on the region, level and model. This is consistent with limitations
213 of coarsely gridded global models in generating small-scale variability in the Tropics
214 (e.g., Willett et al., 2008). The models tend to have the highest variance in the lowest
215 levels (e.g., 925 and 850 hPa), but this behavior holds for AIRS only within DC and at
216 the smallest length scales in other regimes. For SC, the NCAR, C180HIRAM2.1 and
217 MERRA fields show the highest variance at 500 hPa, while ECMWF shows much greater
218 variance at 850 and 925 hPa. However, in most instances, the relative "ordering" of
219 variance by pressure level is consistent between AIRS and the various models.
220 [Figure 1 here]
221 In the case of *q* (Fig. 2), there is a notable absence of a significant scale break in
222 the three regions in the AIRS data (e.g., KT09). The variance is highest for 925 and 850
223 hPa in SC and TC, but not in DC. In fact, the spectral slope of *q* at 925 hPa in DC is
224 much less than that at 850 and 500 hPa. Figure 2 shows the absence of a significant scale
225 break in all models, while the model exponents are uniformly steeper than AIRS. The
226 variance magnitudes are more similar between the models and AIRS in the case of *q* than
227 *T*, although this is less pronounced in the DC region especially for the free-running
228 models that have much too little variance at small scales. The inter-model spread of the
229 variance in the free troposphere (e.g., 500 hPa) is much higher than at 850 and 925 hPa,
230 suggesting bigger discrepancies in the variability of water vapor in the middle
231 troposphere between the models and AIRS observations (c.f., Pierce et al., 2006). In all
232 three regions, the models have a slightly higher magnitude of *q* variance at 850 hPa

compared to 925 hPa presumably from variations in the PBL height that lead to more variations in dry and moist occurrences at a given pressure level. However, this behavior is only observed in DC with AIRS.

[Figure 2 here]

3.2 Zonal averages

Figure 3 shows the zonal averaged T and q exponents for both the large (600–1200 km) and small (150–400 km) scales. All of the models capture some aspects of the zonal structure in T observed by AIRS at the large scales including the decrease in the deep Tropics for T (Nastrom and Gage, 1985; Frehlich and Sharman, 2010). However, the model scaling in the Tropics is uniformly too large, although ECMWF and MERRA have sharper horizontal gradients than CAM3 and C180HIRAM2.1. This is consistent with the inability of convective parameterizations in global models to generate enough small-scale variance from 100–500 km. A scale break in T is observed between the large and small scales, but the small-scale exponents are 0.1–0.3 larger than AIRS. Both ECMWF and MERRA are closer in magnitude to AIRS than CAM3 and C180HIRAM2.1 for large-scale T, but still somewhat higher than AIRS. There is a hint of a decrease in the scaling near the tropopause (Dotzek and Gierens, 2008) in the large T exponents in C180HIRAM2.1, ECMWF and MERRA. However, the CAM3 model has a rather constant increase in the scaling with distance from the Equator and with altitude in large T, while C180HIRAM2.1 has a small peak near 30°N and S, which is even more prominent in ECMWF and MERRA fields. For q scaling, all models show a weak to

256 nonexistent scale break that is consistent with AIRS (KT09) and other limited aircraft
257 observations (Nastrom et al. 1986; Cho et al. 2000). However, the model scaling is still
258 too steep relative to AIRS outside of the tropical troposphere. Furthermore, steeper model
259 exponents are seen near the tropopause and near-surface layers in comparison to AIRS.
260 [Figure 3 here]
261
262 *3.3 SP-CAM and AIRS*
263
264 In Fig. 4, comparisons between SP-CAM and AIRS CWV are shown for three
265 similar regions discussed in Figs. 1 and 2. It is abundantly clear that the scaling in AIRS
266 CWV does not behave like the height-resolved q shown in Figs. 1–3. In fact, CWV has a
267 steeper slope at scales > 250 km in TC and SC compared to DC, much like the scaling of
268 T. Thus, CWV is not an appropriate analogue for layer-resolved q scaling exponents.
269 This emphasizes the importance of making vertically resolved q observations, and sharp
270 differences in boundary layer (0.3) and free troposphere (0.5) exponents obtained from
271 meteorological tower observations support this view (Pressel et al. 2010). The SP-CAM
272 and AIRS have significant differences in both the magnitude of the variances and spectral
273 slopes at scales larger than 100 km, with variations depending on the region, while the
274 SP-CAM is consistently close to 0.3 at smaller scales in all three regions. There is a scale
275 break ~100 km simulated in SP-CAM that is not testable with the current operational
276 AIRS retrieval because of resolution limitations (although future advancements in single
277 AIRS field-of-view retrievals will improve this by a factor of 3). Furthermore, the scaling
278 exponents are more variable between the different years at the larger scales in SP-CAM

compared to the smaller scales, highlighting the importance of monitoring these variations with continuous, multi-year observations of inter-annual variability now available from AIRS.

[Figure 4 here]

Height-resolved q spectra from SP-CAM for the 929, 867, and 600 hPa levels are shown in Fig. 5. The AIRS q spectra for 925, 850, and 500 hPa from Fig. 2 are also shown in Fig. 5 for comparison. The slope of the SP-CAM is much too shallow at all scales, as the slope is essentially flat for all three regions and pressure levels at scales < 250 km, implying scale invariance which is much higher than extrapolation of variance from larger scales. Previous work suggests that the large discrepancy in q variance at small scales may be related to geometrical effects (2D vs. 3D modeling). Moeng et al. (2004) found that 2D simulations of vertical moisture fluxes $\langle w'q' \rangle$ are represented fairly well in comparison to 3D models. Assuming this is also true in the SP-CAM (recall that SP-CAM is a 3D global model with an embedded 2D CRM), vertical moisture fluxes are proportional to correlations between vertical velocity $\langle w'w' \rangle$ and moisture $\langle q'q' \rangle$ variances, thus excessive $\langle q'q' \rangle$ can be compensated by either weaker $\langle w'w' \rangle$ or weaker correlations between $\langle w'w' \rangle$ and $\langle q'q' \rangle$. Modeling comparisons between 2D and 3D CRMs, and a rigorous evaluation of the model variances and fluxes warrants further investigation.

[Figure 5 here]

3.4 VOCALS-REx

In Fig. 6, height-resolved composite spectra of T and q obtained from VOCALS-REx from 30–200 km have spectral slopes similar to AIRS (Fig. 2); however, the slopes are significantly steeper at scales < 10–20 km. The steepening at small scales is reminiscent to slopes steeper than –5/3 observed in boundary layer observations of q reported by Schmitt et al. (1979) and Zhang (2010) and liquid water content (Davis et al., 1996). Furthermore, spectra of T and q obtained from surface buoy data during the East Pacific Investigation of Climate (EPIC) experiment show mesoscale breaks around 20–30 km, although the spectral slopes are less steep than shown in Fig. 6 and are around 0.3–0.5 (Comstock et al., 2005). This is not unexpected as these observations are obtained from a buoy near the surface of the ocean where the scaling is expected to be weaker. All spectra at scales < 10–20 km have increased spectral slopes and are at a minimum for $z <$ 300 m (~0.4) and a maximum for $z >$ 1000 m. The exponents for q are steeper than T in the free troposphere. The T spectra have a scale break ~20 km as with q but is somewhat less pronounced. Since there are a limited number of flight segments at a constant altitude, these composite spectra may not represent the full geophysical variability in this region. However, the distinct change in spectral slopes above and below the inversion base is consistent with AIRS (KT09) and surface-based tower (Pressel et al., 2010) observations. This points to a need for more aircraft observations of thermodynamic variability in the cloudy boundary layer, and data obtained from past aircraft campaigns should be revisited to examine scale-dependent features in T and q.

[Figure 6 here]

4. Discussion and Conclusions

Excessively large fine-scale variability simulated in SP-CAM and observed scale breaks in aircraft data (VOCALS-REx) are located at spatial scales unresolved by current sounders such as AIRS and the Infrared Atmospheric Sounding Interferometer (IASI), or future sounders such as the Cross-Track Infrared Microwave Sounder Suite (CrIMSS), with nominal horizontal resolutions on the order of 50 km. These scale breaks imply that extending variance to smaller scales using exponents obtained from scales resolved by these coarser-resolution sounders may not always be appropriate as suggested by KT09. Observing systems with sufficient spatial resolution (roughly 1–10 km horizontally) that are able to resolve dominant scales of cloud structures (Wood and Field, 2011) are needed to quantify the character of the variability in different cloud regimes for all relevant geophysical variables (Stevens and Feingold, 2009), not only T and q. The problem of extending variance to small scales is highly relevant to promising subgrid-scale cloud parameterization approaches that have not been fully exploited to date (e.g., Cusack et al., 1999; Tompkins, 2002; Kuwano-Yoshida et al., 2010). Small-scale observations are also important for evaluating the new generation of multiscale modeling framework models (e.g., SP-CAM), global CRMs (e.g., Hamilton et al. 2008), and large eddy simulation (LES) models (e.g., Siebesma et al., 2003).

The scaling exponents are found to be steeper in both the free-running models (CAM3 and C180HIRAM2.1) and analyses (ECMWF and MERRA) in comparison to AIRS, suggesting that the small-scale variance in these models is too small. It is not known whether this behavior is driven (in part, or in whole) by differences in parameterizations (e.g., Hamilton et al., 2008), data assimilation (satellite, radiosonde,

348 and surface observations), or other reasons, and warrants further investigation. However,
349 it appears that the free-running models used in climate assessments are not as complete in
350 resolving the scale dependence of T and q variance than models with 3-D or 4-DVAR
351 systems (e.g., ECMWF and MERRA). This is qualitatively consistent with slightly
352 poorer performance of climate models that are executed in 'weather forecast mode' when
353 compared to NWP models (Phillips et al., 2004), however, small-scale variability may
354 not be the main factor in these differences of forecast skill. More research is necessary to
355 determine the potential implications for climate sensitivity and cloud feedback sign and
356 magnitude, which include tests of ECMWF and MERRA without realistic initialization.
357 Additional studies such as Cusack et al. (1999) should be undertaken that use constraints
358 on subgrid-scale variability obtained from observations. As the SP-CAM results indicate,
359 having embedded CRMs that serve as subgrid-scale parameterizations does not
360 necessarily ensure realistic q spectra. Observational constraints from satellite and aircraft
361 observations will play an important role in parameterization efforts.

362 This work shows that higher horizontal spatial resolution observations of T and q
363 over the entire globe are necessary to observe the global characteristics of "turbulence" in
364 thermodynamic profiles. At the same time, current and future operational and research
365 atmospheric sounders will continue to play a role in assessing climate processes,
366 establishing quantitative benchmarks for model comparisons, facilitate the development
367 of more rigorous observationally-based subgrid-scale parameterizations, and possibly
368 offer a long-term strategy to monitor the mesoscale spectrum of T and q on a global basis.
369 As shown by Hamilton et al. (2008), the observed KE spectrum serves as a useful
370 diagnostic for climate model assessments. We suggest that height- and regime-resolved

371 spectra of T and q should also be included in model diagnostics as they can be highly
372 variable in space and time. Additional A-train data sets can serve as benchmarks for other
373 model-relevant variables such as cloud water content and precipitation, and their
374 simultaneous observation with T and q can be combined into multi-sensor observational
375 estimates of moist conserved thermodynamic variables that directly "interface" with
376 model parameters.
377
378 **Acknowledgments.** Support from the JPL Internal Research and Technology
379 Development Program, NASA's Making Earth Science Data Records for Use in Research
380 Environments (MEaSUREs) program, and the AIRS Project at JPL is acknowledged. The
381 work of X. L. Huang is partly supported by NSF grant ATM0755310. AIRS data were
382 obtained through the Goddard Earth Sciences Data and Information Services Center
383 (http://daac.gsfc.nasa.gov/). ECMWF data are provided in coordination with the Year of
384 Coordinated Observing Modeling and Forecasting Tropical Convection project
385 (http://data-portal.ecmwf.int/data/d/yotc_od/). MERRA data are provided by the Global
386 Modeling and Assimilation Office (http://gmao.gsfc.nasa.gov/). This material is partly
387 based upon work supported by the National Science Foundation Science and Technology
388 Center for Multi-Scale Modeling of Atmospheric Processes, managed by Colorado State
389 University under cooperative agreement No. ATM-0425247. Roger Marchand provided
390 the SP-CAM output. The MMF model runs were performed at the Department of Energy
391 Pacific Northwest National Laboratory (PNNL) and the San Diego Supercomputing
392 Center (SDSC). This research was carried out at the Jet Propulsion Laboratory, California
393 Institute of Technology, under a contract with NASA.
394

394

395 **References**

396

397 Aumann, H. H., and Coauthors, 2003: AIRS/AMSU/HSB on the Aqua mission: Design,
398 science objectives, data products, and processing systems. *IEEE Trans. Geosci. Remote*
399 *Sens*., **41**, 253–264.

400

401 Bony, S., and J. L. Dufresne, 2005: Marine boundary layer clouds at the heart
402 of tropical cloud feedback uncertainties in climate models. *Geophys. Res. Lett*.,
403 **32**, L20806, doi:10.1029/2005GL023851.

404

405 Cahalan, R. F., W. Ridgway, W. J. Wiscombe, and T. L. Bell, 1994: The albedo of fractal
406 stratocumulus clouds. *J. Atmos. Sci*., **51**, 2434–2455.

407

408 Cho, J. Y. N., R. E. Newell, and G. W. Sachse, 2000: Anomalous scaling of mesoscale
409 troposheric humidity fluctuations. *Geophys. Res. Lett*., **27**, 377–380.

410

411 Comstock, K. K., C. S. Bretherton, and S. E. Yuter, 2005: Mesoscale variability and
412 drizzle in southeast Pacific stratocumulus. *J. Atmos., Sci*., **62**, 3792–3807.

413

414 Cusack, S., J. M. Edwards, and R. Kershaw, 1999: Estimating the subgrid variance of
415 saturation, and its parameterization for use in a GCM cloud scheme. *Q. J. Royal. Met.*
416 *Soc*., **125**, 3057–3076.

Davis, A. B., A. Marshak, W. Wiscombe, and R. Cahalan, 1996: Scale invariance of liquid water distributions in marine stratocumulus. Part I: Spectral properties and stationarity issues. *J. Atmos. Sci*., **53**, 1538–1558.

Dotzek, N., and K. Gierens, 2008: Instantaneous fluctuations of temperature and moisture in the upper troposphere and tropopause region. Part 2: Structure functions and intermittency. *Meteor. Z*., **16**, 221–231.

Fetzer, E. J., B. H. Lambrigtsen, A. Eldering, H. H. Aumann, and M. T. Chahine, 2006: Biases in total precipitable water vapor climatologies from Atmospheric Infrared Sounder and Advanced Microwave Scanning Radiometer. *J. Geophys. Res*., **111**, D09S16, doi:10.1029/2005JD006598, 2006. 19, 1388–1406, 2006.

Frehlich, R., and R. Sharman, 2010: Climatology of velocity and temperature turbulence statistics determined from rawinsonde and ACARS/AMDAR data. *J. Appl. Meteor. Climatol*., **49**, 1149–1169.

Gettelman, A., X. Liu, S. J. Ghan, H. Morrison, S. Park, A. J. Conley, S. A. Klein, J. Boyle, D. L. Mitchell, and J-L. F. Li, 2010: Global simulations of ice nucleation and ice supersaturation with an improved cloud scheme in the Community Atmosphere Model. *J. Geophys. Res.*, 115, D18216, doi:10.1029/2009JD013797.

GFDL GAMDT, 2004: The New GFDL global atmosphere and land model AM2–LM2: Evaluation with prescribed SST simulations. *J. Climate*, **17**, 4641–4673.

Hamilton, K., Y. O. Takahashi, and W. Ohfuchi, 2008: The mesoscale spectrum of atmospheric motions investigated in a very fine resolution global general circulation model. *J. Geophys. Res*., **113**, D18110, doi:10.1029/2008JD009785.

Jung, T., G. Balsamo, P. Bechtold, A. C. M. Beljaars, M. Köhler, M. J. Miller, J.-J. Morcrette, A. Orr, M. J. Rodwell, and A. M. Tompkins, 2010: The ECMWF model climate: Recent progress through improved physical parameterizations. *Q. J. Royal. Met. Soc*., **136**, 1145–1160, doi:10.1002/qj.634.

Kahn, B. H., and J. Teixeira, 2009: A global climatology of temperature and water vapor variance scaling from the Atmospheric Infrared Sounder. *J. Climate*, 22, 5558–5576, doi: 10.1175/2009JCLI2934.1.

Kawai, H., and J. Teixeira, 2010: Probability density functions of liquid water path and cloud amount of marine boundary layer clouds: Geographical and seasonal variations and controlling meteorological factors. *J. Climate*, **23**, 2079–2092.

Koshyk, J. N., K. Hamilton, and J. D. Mahlman, 1999: Simulation of the $k^{-5/3}$ mesoscale spectral regime in the GFDL SKYHI general circulation model. *Geophys. Res. Lett*., **26**, 843–846.

463

464 Kuwano-Yoshida, A., T. Enomoto, and W. Ohfuchi, 2010: An improved PDF cloud
465 scheme for climate simulations. *Q. J. Royal. Met. Soc*., **136**, 1583–1597,
466 doi:10.1002/qj.660.
467
468 Lindborg, E., 2009: Two comments on the surface quasigeostrophic model for the
469 atmospheric energy spectrum. *J. Atmos. Sci*., **66**, 1069–1072.
470
471 Lindborg, E., K. K. Tung, G. D. Nastrom, J. Y. N. Cho, and K. S. Gage, 2009: Comment
472 on "Reinterpreting aircraft measurement in anisotropic scaling turbulence" by Lovejoy et
473 al. (2009). *Atmos. Chem. Phys*., **10**, 1401–1402.
474
475 Lovejoy, S. A. F. Tuck, D. Schertzer, and S. J. Hovde, 2009: Reinterpreting aircraft
476 measurements in anisotropic scaling turbulence. *Atmos. Chem. Phys*., **9**, 5007–5025.
477
478 Maddy, E. S., and C. D. Barnet, 2008: Vertical resolution estimates in version 5 of AIRS
479 operational retrievals. *IEEE Trans. Geosci. Remote Sens*., **46**, 2375–2384.
480
481 Marchand, R., N. Beagley, and T. P. Ackerman, 2009: Evaluation of hydrometeor
482 occurrence profiles in the Multiscale Modeling Framework climate model using
483 atmospheric classification. *J. Climate*, **22**, 4557–4573, doi:10.1175/2009JCLI2638.1
484

485 Moeng, C.-H., J. C. McWilliams, R. Rotunno, P. P. Sullivan, and J. Weil, 2004:
486 Investigating 2D modeling of atmospheric convection in the PBL. *J. Atmos. Sci*., **61**,
487 889–903.
488
489 Nastrom, G. D., and K. S. Gage, 1985: A climatology of atmospheric wavenumber
490 spectra of wind and temperature observed by commercial aircraft. *J. Atmos. Sci*., **42**,
491 950–960.
492
493 Nastrom, G. D., W. H. Jasperson, and K. S. Gage, 1986: Horizontal spectra of
494 atmospheric tracers measured during the global atmospheric sampling program. *J.*
495 *Geophys. Res*., **91**, 13,201–13,209.
496
497 Phillips, T. J., G. L. Potter, D. L. Williamson, R. T. Cederwall, J. S. Boyle, M. Fiorino, J.
498 J. Hinto, J. G. Olsen, S. Xie, and J. J. Yio, 2004: Evaluating parameterizations in general
499 circulation models: Climate simulation meets weather prediction. *Bull. Amer. Met. Soc*.,
500 **85**, 1903–1915.
501
502 Pierce, D. W., T. P. Barnett, E. J. Fetzer, and P. J. Gleckler, 2006: Three-dimensional
503 tropospheric water vapor in coupled climate models compared with observations from the
504 AIRS satellite system. *Geophys. Res. Lett.*, **33**, L21701, doi:10.1029/2006GL027060.
505
506 Pressel, K. G., W. D. Collins, and A. R. Desal, 2010: Variance scaling in water vapor
507 measurements from a tall tower. Preprints, 13th Conf. on Cloud Physics, Portland, OR,

508 Amer. Met. Soc., P.1777 [Available online at:
509 http://ams.confex.com/ams/13CldPhy13AtRad/techprogram/paper-171839.htm]
510
511 Randall, D. A., et al., 2007: Climate models and their evaluation, in *Climate Change*
512 *2007: The Physical Science Basis. Contribution of Working Group I to the Fourth*
513 *Assessment Report of the Intergovernmental Panel on Climate Change*, edited by S.
514 Solomon et al., pp. 589–662, Cambridge University Press, Cambridge, U. K.
515
516 Rienecker, M. M., M. J. Suarez, R. Todling, J. Bacmeister, L. Takacs, H.-C. Liu, W. Gu,
517 M. Sienkiewicz, R. D. Koster, R. Gelaro, I. Stajner, and J. E. Nielsen, 2008: The GEOS-5
518 data assimilation system – Documentation of Versions 5.0.1, 5.1.0, and 5.2.0. NASA
519 Technical Report, TM-2008-104606, Vol. 27, 118 pp.
520
521 Schmitt, K. F., C. A. Friehe, and C. H. Gibson, 1979: Structure of marine surface layer
522 turbulence. *J. Atmos. Sci*., **36**, 602–618.
523
524 Siebesma, A. P., C. S. Bretherton, A. Brown, A. Chlond, J. Cuxart, P. G. Duynkerke, H.
525 Jiang, M. Khairoutdinov, D. Lewellen, C.-H. Moeng, E. Sanchez, B. Stevens, and D. E.
526 Stevens, 2003: A large eddy simulation intercomparison study of shallow cumulus
527 convection. *J. Atmos., Sci*., **60**, 1201–1219.
528
529 Skamarock, W. C., 2004: Evaluating mesoscale NWP models using kinetic energy
530 spectra. *Mon. Wea. Rev*., **132**, 3019–3032.

Smith, K. S., and R. Tulloch, 2009: Reply. *J. Atmos. Sci*., **66**, 1073–1076.

Stevens, B., and G. Feingold, 2009: Untangling aerosol effects on clouds and precipitation in a buffered system. *Nature*, **461**, 607–613.

Susskind, J., C. D. Barnet, and J. M. Blaisdell, 2003: Retrieval of atmospheric and surface parameters from AIRS/AMSU/HSB data in the presence of clouds. *IEEE Trans. Geosci. Remote Sens*., **41**, 390–409.

Takahashi, Y. O., K. Hamilton, and W. Ohfuchi, 2006: Explicit global simulation of the mesoscale spectrum of atmospheric motions. *Geophys. Res. Lett*., **33**, L12812, doi:10.1029/2006GL026429.

Tompkins, A. M., 2002: A prognostic parameterization for the sub-grid scale variability of water vapor and clouds in large-scale models and its use to diagnose cloud cover. *J. Atmos. Sci*., **59**, 1917–1942.

Tuck, A. F., 2010: From molecules to meteorology via turbulent scale invariance. *Q. J. Royal. Met. Soc*., **136**, 1125–1144, doi:10.1002/qj.644.

552 Tulloch, R., and K. S. Smith, 2006: A theory for the atmospheric energy spectrum:
553 Depth-limited temperature anomalies at the tropopause. *Proc. Natl. Academy. Sci*., **103**,
554 14690–14694.
555
556 Tung, K. K., and W. W. Orlando, 2003: The k^{-3} and $k^{-5/3}$ energy spectrum of atmospheric
557 turbulence: Quasigeostrophic two-level model simulation. *J. Atmos. Sci*., **60**, 824–835.
558
559 Wang, H., G. Feingold, R. Wood, and J. Kazil, 2010: Modelling microphysical and
560 meteorological controls on precipitation and cloud cellular structures in Southeast Pacific
561 stratocumulus. *Atmos. Chem. Phys*., **10**, 6347–6362.
562
563 Willett, M. R., P. Bechtold, D. L. Williamson, J. C. Petch, S. F. Milton, and S. J.
564 Woolnough, 2008: Modeling suppressed and active convection: Comparisons between
565 three global atmospheric models. *Q. J. Royal. Met. Soc*., **134**, 1881–1896,
566 doi:10.1002/qj.317.
567
568 Wood, R., and D. L. Hartmann, 2006: Spatial variability of liquid water path in marine
569 low cloud: The importance of mesoscale cellular convection. *J. Climate*, **19**, 1748–1764.
570
571 Wood, R., C. S. Bretherton, D. Leon, A. D. Clarke, P. Zuidema, G. Allen, and H. Coe,
572 2010: An aircraft case study of the spatial transition from closed to open mesoscale
573 cellular convection over the Southeast Pacific. *Atmos. Chem. Phys. Discuss*., **10**, 17911–
574 17980.

Wood, R., and P. R. Field, 2011: The distribution of cloud horizontal sizes. Submitted to *J. Climate*

Zhang, J. A., 2010: Spectral characteristics of turbulence in the hurricane boundary layer over the ocean between the outer rain bands. *Q. J. Royal Met. Soc*., **136**, 918–926, doi:10.1002/qj.610.

Zhao, M., I. M. Held, S.-J. Lin, and G. A. Vecchi, 2009: Simulations of global hurricane climatology, inter-annual variability, and response to global warming using a 50-km resolution GCM. *J. Climate*, **22**, 6653–6678, doi:10.1175/2009JCLI3049.1.

587

588 Table 1. Summary of weather and climate models: spatial resolution/grid configuration,

589 data assimilation constraints, and the simulation period.

590

Model	Horizontal Resolution	Output Fields	Data assimilation?	Simulation Period
GFDL C180HIRAM2.1	0.5° × 0.625°	Same	NO	01 Sept. 1995 – 30 Nov. 1995
NCAR CAM3	0.31° × 0.23°	Same	NO	01 June 2005 – 31 Aug. 2005
ECMWF (CY35R2)	0.25° × 0.25°	0.5° × 0.5°	YES	01 June 2009 – 31 Aug. 2009
MERRA	0.5° × 0.625°	1.25° × 1.25°	YES	01 June 2009 – 31 Aug. 2009
SP-CAM	2.5° × 2.0° Embedded 2D CRM with 64 columns of 4 km resolution	Same	NO	01 Sept. – 30 Nov. for the years 1998– 2001

591

592

592

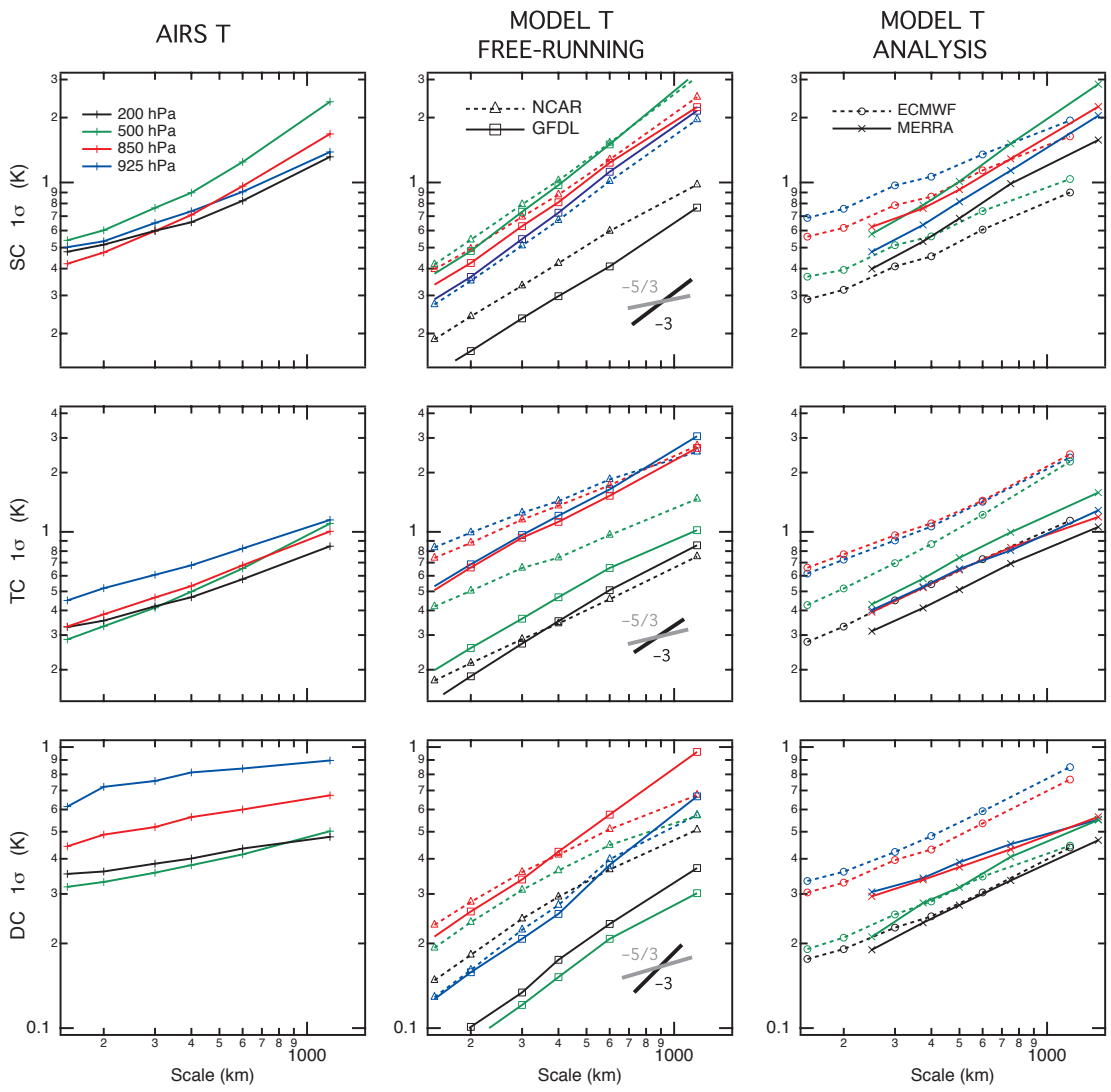

593

594

595 Figure 1. Variance spectra of *T* for three spatial regions: SE Pacific stratocumulus region

596 [24°S, 90°W(97.5°W)], trade cumulus near Hawaii [24°N, 150°W(157.5°W)], and

597 convective region in tropical Western Pacific [0°, 150°E(157.5°E)]. AIRS, ECMWF and

598 CAM3 (C180HIRAM2.1) model results contained within a 12°×12° (12°×15°) box

599 centered at first (second) longitudinal value.

600

600

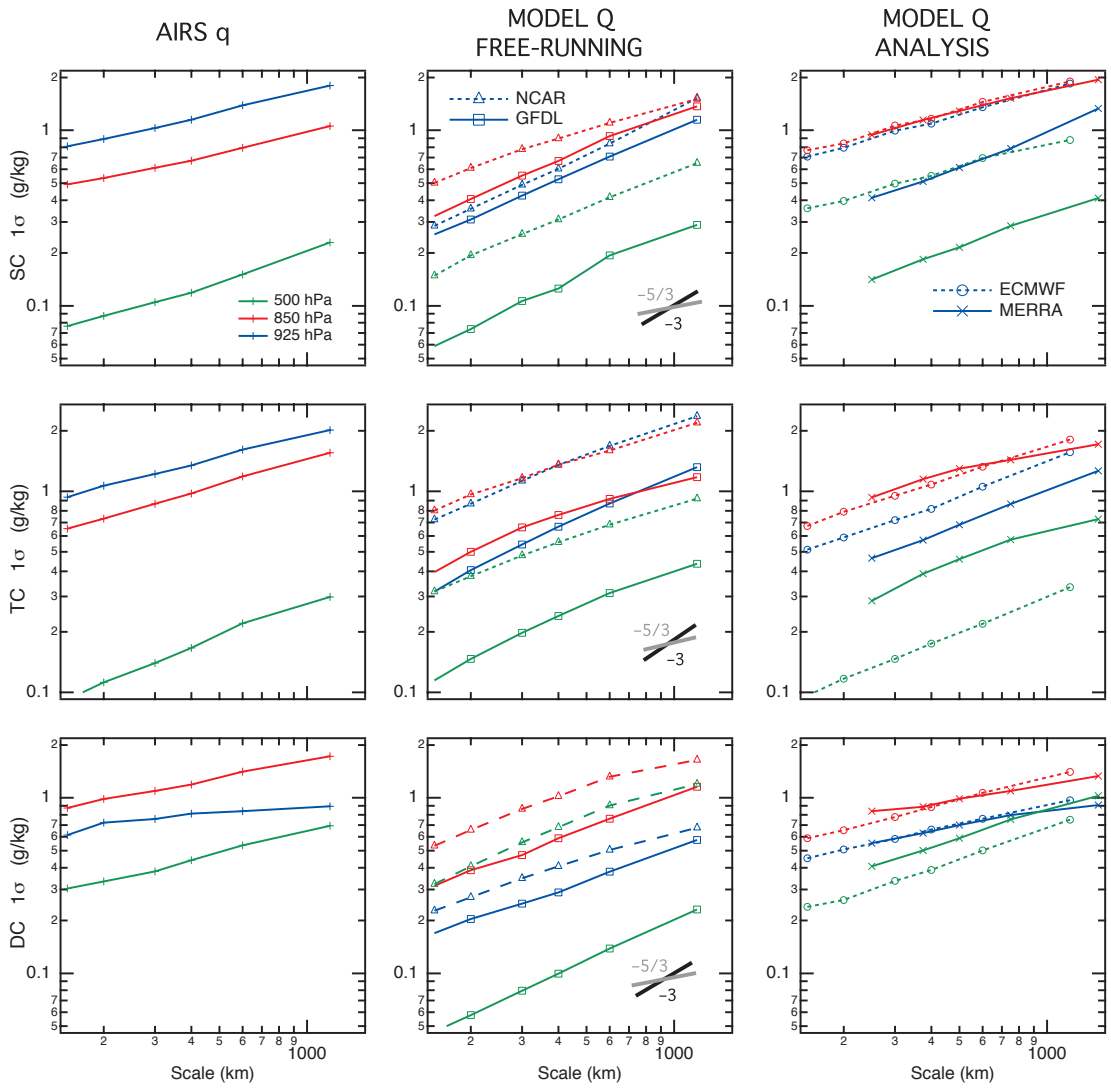

601

602 Figure 2. All panels identical to Fig. 1 but for the quantity *q* (g/kg).

603

604

604

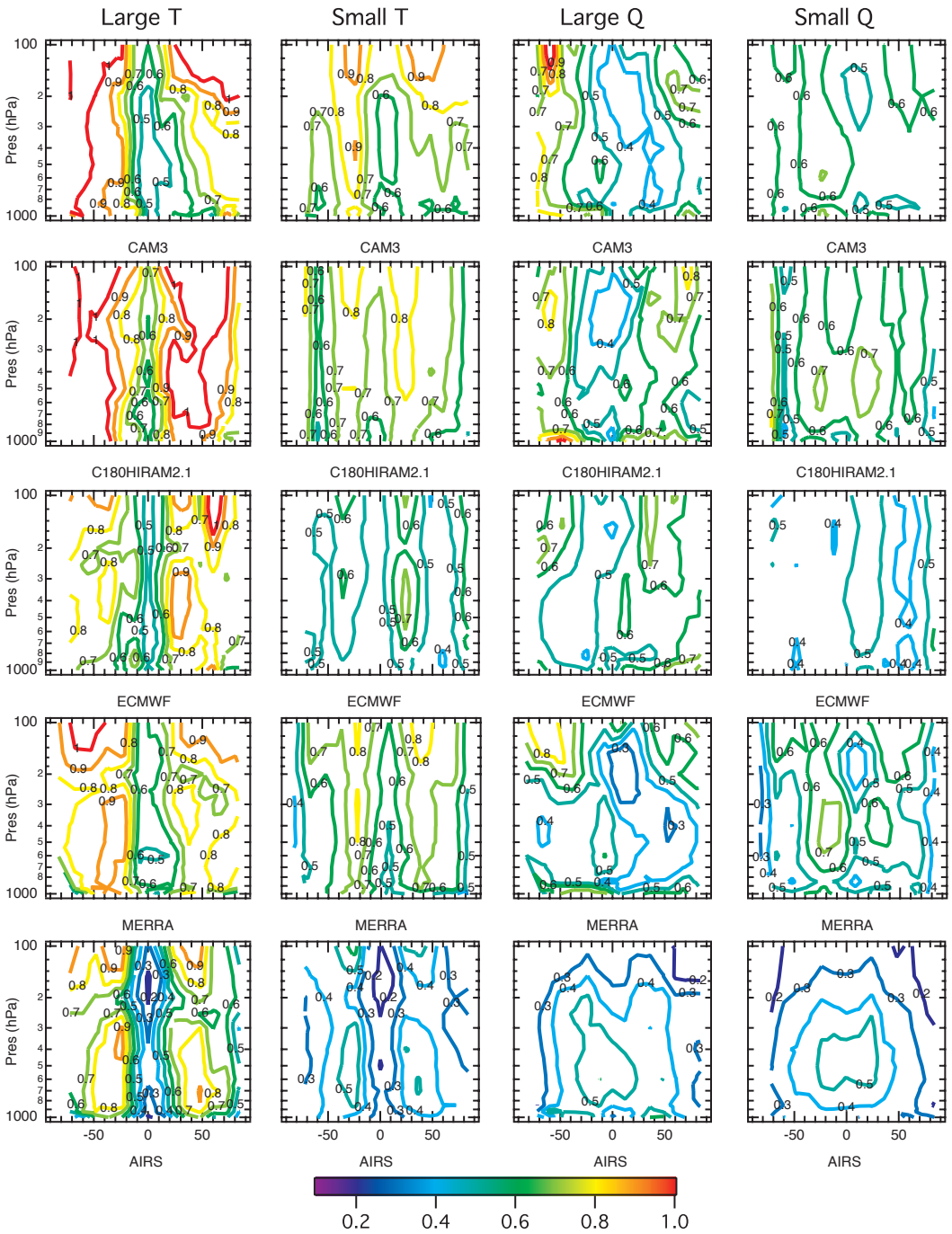

605
606

607 Figure 3. Zonal averaged scaling exponents for AIRS, MERRA, ECMWF,

608 C180HIRAM2.1 and CAM3 *T* (left two columns) and *q* (right two columns) for "clear

609 sky" (see text for a description). The large (small) exponents are obtained from fitting

power law exponents restricted to 600–1200 km (150–400 km) following the methodology of *KT09*, except for MERRA, which are obtained from 250–500 km (750–1500 km).

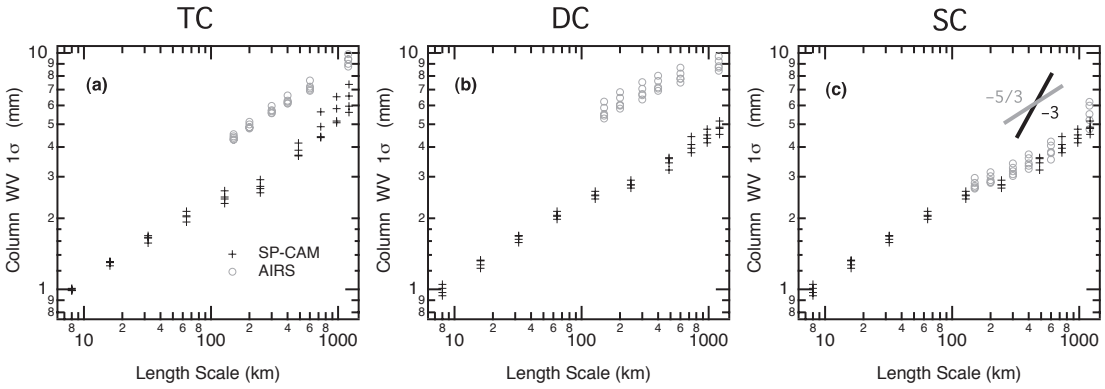

Figure 4. Shown are CWV spectra of SP-CAM (AIRS) for three regions: (a) 157.5°–170°W and 10°–20°N (156°–168°W and 6°–18°N), (b) 157.5°–170°E and 4°S–6°N (150°–162.5°E and 6°S–6°N), and (c) 77.5°–90°W and 10°–20°S (84°–96°W and 6°–18°S) (right). All spectra are from SON at 12Z during 1998–2001 (SP-CAM) and 0Z during 2004–2008 (AIRS). The scaling exponents for –5/3 (0.33) and –3 (1.0) are shown in gray (black).

623

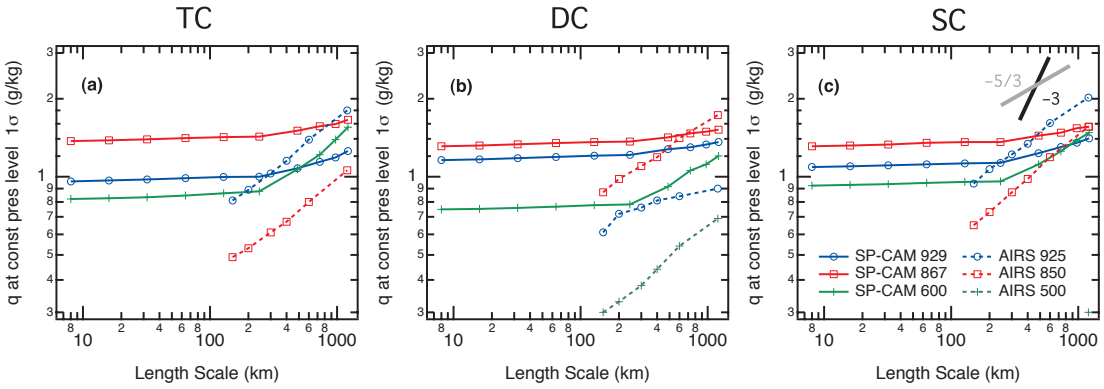

624

625 Figure 5. Similar to Fig. 4 except 1σ values of *q* shown at constant pressure levels in SP-

626 CAM and AIRS.

627

628

628

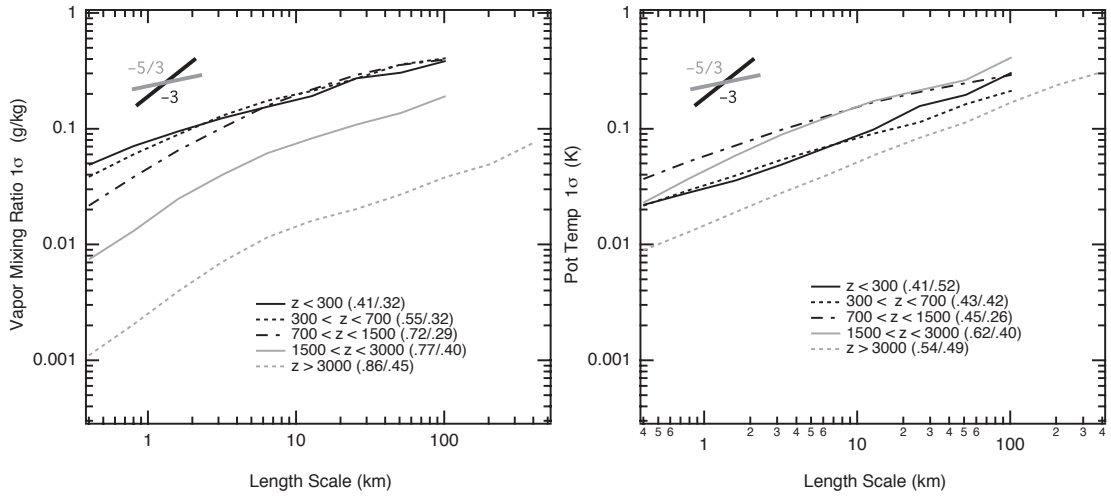

629

630 Figure 6. Shown are composite variance spectra for q (left) and θ (right) in five altitude
631 bins during VOCALS-REx for flight segments with at least five segments averaged (see
632 text). The numbers in the parentheses are scaling exponents for spectra < 10 km on the
633 left (> 10 km on the right).

634

635